

**“Silicon-based visible/near infrared affordable missile warning”
Contract: N00014-03-M-0308**

**Option Phase Final Report
CLIN No. 0002AB
January 1, 2005**

I. Introduction

The concept of the refluorescent atomic filter is shown in figure 2. Only photons at the resonant frequency of the atomic transition line are absorbed; all other photons pass through the cell without interference. If the atomic vapor is optically thick on the resonance absorption line, then photons absorbed by the atoms are trapped within the optical depth the entrance window of the cell. This trapping occurs at the same wavelength independent of the angle at which the photons arrive. In the absence of quenching, these photons undergo a random walk as they are absorbed and emitted the potassium atoms. Since the mean free path is only a few microns, the trapped photons finally exit the cell in the backward direction, through the entrance window. In this manner, the cell appears as a Lambertian scatterer for light within the absorption bandwidth. As with any Lambertian scatterer, the illumination can come from any direction, so the potassium filter has an acceptance angle of up to 2π steradians. This feature is in contrast to narrow linewidth interference filters and etalons, which can only accept light over a very narrow entrance angle and are thus not useful for this wide angle application.

The conceptual design of the WMS using a potassium vapor cell is shown in figure 3. The emission of the missile plume is collected by an optical system and imaged onto the surface of the potassium vapor cell. All background optical signals including the solar background will pass through the vapor cell and be dumped. Only the potassium light emission from the plume at the potassium D lines will be trapped at the surface and form an image. A beam splitter or equivalent method is used to separate the entering photons and reemitted photons, and a low f number lens is used to collect these reemitted photons and image them onto a CCD.

II. Potassium Cell Absorption

If a beam of monochromatic light propagates through an atomic gas with length L , the transmitted intensity is given by Beer's Law:

$$I_{out} = I_{in} e^{-\alpha(\nu)L}$$

where I_{out} and I_{in} are the transmitted and input light intensity respectively, and $\alpha(\nu)$ is the absorption coefficient at frequency ν . Considering the hyperfine structure of the potassium D transitions, the absorption coefficient is the summation of all hyperfine structure transition contributions:

$$\alpha(\nu) = \frac{e^2}{4\epsilon_0 m_e c} \sum_i N_i f_i V(\nu_i)$$

where N_i is the number density of a specific isotope, f_i is the oscillator strength, and $V(\nu_i)$ is the normalized Voigt line shape function for the specific hyperfine transition.

Potassium has two well known resonance lines to the ground state, the D2 line: $4P_{3/2} \rightarrow 4S_{1/2}$ and the D1 line: $4P_{1/2} \rightarrow 4S_{1/2}$. The transition probabilities of these two lines are approximately the same: $A_{D2} = 3.87 \times 10^7 \text{ s}^{-1}$, $A_{D1} = 3.87 \times 10^7 \text{ s}^{-1}$. But the oscillator strengths are not. The oscillator strength f can be calculated from the following equation:

REPORT DOCUMENTATION PAGE

*Form Approved
OMB No. 0704-0188*

The public reporting burden for this collection of information is estimated to average 1 hour per response, including the time for reviewing instructions, searching existing data sources, gathering and maintaining the data needed, and completing and reviewing the collection of information. Send comments regarding this burden estimate or any other aspect of this collection of information, including suggestions for reducing the burden, to Department of Defense, Washington Headquarters Services, Directorate for Information Operations and Reports (0704-0188), 1215 Jefferson Davis Highway, Suite 1204, Arlington, VA 22202-4302. Respondents should be aware that notwithstanding any other provision of law, no person shall be subject to any penalty for failing to comply with a collection of information if it does not display a currently valid OMB control number.

PLEASE DO NOT RETURN YOUR FORM TO THE ABOVE ADDRESS.

1. REPORT DATE (DD-MM-YYYY)			2. REPORT TYPE		3. DATES COVERED (From - To)	
4. TITLE AND SUBTITLE				5a. CONTRACT NUMBER		
				5b. GRANT NUMBER		
				5c. PROGRAM ELEMENT NUMBER		
6. AUTHOR(S)				5d. PROJECT NUMBER		
				5e. TASK NUMBER		
				5f. WORK UNIT NUMBER		
7. PERFORMING ORGANIZATION NAME(S) AND ADDRESS(ES)				8. PERFORMING ORGANIZATION REPORT NUMBER		
9. SPONSORING/MONITORING AGENCY NAME(S) AND ADDRESS(ES)				10. SPONSOR/MONITOR'S ACRONYM(S)		
				11. SPONSOR/MONITOR'S REPORT NUMBER(S)		
12. DISTRIBUTION/AVAILABILITY STATEMENT						
13. SUPPLEMENTARY NOTES						
14. ABSTRACT						
15. SUBJECT TERMS						
16. SECURITY CLASSIFICATION OF:			17. LIMITATION OF ABSTRACT	18. NUMBER OF PAGES	19a. NAME OF RESPONSIBLE PERSON	
a. REPORT	b. ABSTRACT	c. THIS PAGE			19b. TELEPHONE NUMBER (Include area code)	

INSTRUCTIONS FOR COMPLETING SF 298

1. REPORT DATE. Full publication date, including day, month, if available. Must cite at least the year and be Year 2000 compliant, e.g. 30-06-1998; xx-06-1998; xx-xx-1998.

2. REPORT TYPE. State the type of report, such as final, technical, interim, memorandum, master's thesis, progress, quarterly, research, special, group study, etc.

3. DATES COVERED. Indicate the time during which the work was performed and the report was written, e.g., Jun 1997 - Jun 1998; 1-10 Jun 1996; May - Nov 1998; Nov 1998.

4. TITLE. Enter title and subtitle with volume number and part number, if applicable. On classified documents, enter the title classification in parentheses.

5a. CONTRACT NUMBER. Enter all contract numbers as they appear in the report, e.g. F33615-86-C-5169.

5b. GRANT NUMBER. Enter all grant numbers as they appear in the report, e.g. AFOSR-82-1234.

5c. PROGRAM ELEMENT NUMBER. Enter all program element numbers as they appear in the report, e.g. 61101A.

5d. PROJECT NUMBER. Enter all project numbers as they appear in the report, e.g. 1F665702D1257; ILIR.

5e. TASK NUMBER. Enter all task numbers as they appear in the report, e.g. 05; RFO330201; T4112.

5f. WORK UNIT NUMBER. Enter all work unit numbers as they appear in the report, e.g. 001; AFAPL30480105.

6. AUTHOR(S). Enter name(s) of person(s) responsible for writing the report, performing the research, or credited with the content of the report. The form of entry is the last name, first name, middle initial, and additional qualifiers separated by commas, e.g. Smith, Richard, J, Jr.

7. PERFORMING ORGANIZATION NAME(S) AND ADDRESS(ES). Self-explanatory.

8. PERFORMING ORGANIZATION REPORT NUMBER. Enter all unique alphanumeric report numbers assigned by the performing organization, e.g. BRL-1234; AFWL-TR-85-4017-Vol-21-PT-2.

9. SPONSORING/MONITORING AGENCY NAME(S) AND ADDRESS(ES). Enter the name and address of the organization(s) financially responsible for and monitoring the work.

10. SPONSOR/MONITOR'S ACRONYM(S). Enter, if available, e.g. BRL, ARDEC, NADC.

11. SPONSOR/MONITOR'S REPORT NUMBER(S). Enter report number as assigned by the sponsoring/monitoring agency, if available, e.g. BRL-TR-829; -215.

12. DISTRIBUTION/AVAILABILITY STATEMENT. Use agency-mandated availability statements to indicate the public availability or distribution limitations of the report. If additional limitations/ restrictions or special markings are indicated, follow agency authorization procedures, e.g. RD/FRD, PROPIN, ITAR, etc. Include copyright information.

13. SUPPLEMENTARY NOTES. Enter information not included elsewhere such as: prepared in cooperation with; translation of; report supersedes; old edition number, etc.

14. ABSTRACT. A brief (approximately 200 words) factual summary of the most significant information.

15. SUBJECT TERMS. Key words or phrases identifying major concepts in the report.

16. SECURITY CLASSIFICATION. Enter security classification in accordance with security classification regulations, e.g. U, C, S, etc. If this form contains classified information, stamp classification level on the top and bottom of this page.

17. LIMITATION OF ABSTRACT. This block must be completed to assign a distribution limitation to the abstract. Enter UU (Unclassified Unlimited) or SAR (Same as Report). An entry in this block is necessary if the abstract is to be limited.

$$f_{ij} = \frac{g_j}{g_i} \frac{8\pi^2 m_e \epsilon_0 c \lambda^2 A_{ji}}{2\pi e^2}$$

Since $g_{S1/2}=2$, $g_{P3/2}=4$, $g_{P1/2}=2$, f is $2/3$ for D2 line, f is $1/3$ for D1 line. So the absorption coefficient of the D2 transition is twice as large as the D1 transition, and thus the optical depth is shorter by a factor of two. From this point of view the D2 lines is the better choice for the optical filter. In the following, the modeling and experiments are restricted to the D2 transition of K atom.

There are three naturally occurring isotopes of K: ^{39}K , ^{41}K and ^{40}K . Their natural abundances are ^{39}K 93.26%, ^{41}K 6.73%, ^{40}K 0.012%. If we use the transitions of ^{39}K as the reference, the isotopic shifts for other isotopes are: ^{41}K : 236.15 MHz, and ^{40}K : 126.43 MHz [7]. Different isotopes also have different nuclear spins: ^{39}K : $I=3/2$, ^{41}K : $I=3/2$, ^{40}K : $I=4$. Because the natural abundance of ^{40}K is comparably small, it is neglected in the modeling.

The hyperfine energy shift due to the nuclear spin orbital angular momentum coupling is given by:

$$\Delta E_{hfs} = \frac{hCA}{2} + hB \frac{\frac{3}{2}C(C+1) - 2I(I+1)J(J+1)}{2I(2I-1)2J(2J-1)}$$

where $C = F(F+1) - I(I+1) - J(J+1)$, F is the total angular momentum and h is the Planck's constant, I is the nuclear spin, and A and B are the hyperfine interaction constant for each state. The two terms in the equation originate from the magnetic dipole and the electrical quadruple interaction respectively. The value of the coupling constants A and B are given in reference [8]. The relative wavelength and strength of all the D2 transitions included in the model are plotted in figure 4.

It can be seen from Figure 4 that the splittings of the hyperfine lines are all less than 1 GHz, which is quite different from rubidium (~ 10 GHz) and mercury (~ 30 GHz).

The absorption profile is then found from the summation of the broadened hyperfine lines. The three broadening mechanism considered in the model are thermal broadening, natural broadening and collisional self broadening. The broadening due to atomic thermal motion contributes an inhomogeneous Gaussian component:

$$G(\nu) = \frac{1}{\sqrt{\pi} \Delta \nu_g} \exp \left[- \left(\frac{\nu - \nu_0}{\Delta \nu_g} \right)^2 \right]$$

where

$$\Delta \nu_g = \frac{\nu_0}{c} \sqrt{\frac{2k_B T}{m_K}}$$

is the Gaussian-component width. At our experiment condition, the body of the K cell is kept at $T=200^\circ\text{C}$, which gives us the $\Delta \nu_g \sim 700$ MHz. Because the hyperfine splitting is on the order of $100 \sim 200$ MHz, with 700 MHz thermal broadening, hyperfine lines will not be seen separately in the measured absorption profiles.

The natural broadening and collisional self broadening both combine to form a homogeneous Lorentzian profile.

$$L(\nu) = \frac{1}{\pi} \frac{\frac{\Delta \nu_L}{2}}{(\nu - \nu_0)^2 + \left(\frac{\Delta \nu_L}{2}\right)^2}$$

where $\Delta \nu_L = \Delta \nu_N + \Delta \nu_S$. Natural broadening $\Delta \nu_N = 2\pi/A_{ij} = 6.16 \text{ MHz}$. Collisional self broadening is $\Delta \nu_S = K_{sb}N$, where N is the number density of K atoms. The self-broadening coefficient K_{sb} can be found in reference [9].

The combination of the Gaussian component and Lorentzian component is a Voigt function.

$$V(\nu) = \int_{-\infty}^{\infty} G(\nu')L(\nu - \nu')d\nu'$$

For simplification of the calculation of the Voigt profile, the Whiting approximation is used [10]. The essence of the Whiting approximation is an empirical approximation by a single equation, and the error is predicted to be -5%~+2% within 10 $\Delta \nu_g$. The result of the modeling is plotted in figure 5 together with the experimental results.

In absorption experiments, a Sacher TEC-500-765-10 External Cavity Diode Laser was used as the light source. The Sacher laser has an output power of approximately 10 mW and a linewidth of less than 1 MHz. It has an electronically controllable frequency tuning range of approximately 250 GHz by changing the voltage on a piezo-electric actuator. Continuous frequency tuning is achieved over about 10 GHz. Beyond this range, there is a discontinuity in the frequency due to laser mode hopping. The laser also has a coarse tuning range of approximately 10 nm that is achieved by tuning the screw on the laser head.

The potassium vapor cell used in this experiment consists with a cylindrical cell body and a cold tip. The length of the cell body is 5 cm. Both parts are heated, the body temperature is kept at 200 °C, and the tip temperature of the cell is used to control the potassium vapor pressure.

The absorption profiles are measured at different tip temperatures. The potassium vapor pressure can be calculated for the various tip temperatures [11].

T_{tip} (°C)	30	60	100
Pressure (torr)	3.6×10^{-8}	7.5×10^{-7}	2.0×10^{-5}

The measurement results are plotted in figure 5. The modeling matches experimental result almost perfectly. Note that the Full width at Half maximum bandwidth of the absorption profile increases with the increase of potassium vapor pressure, from 0.5 GHz at 30 °C to 3 GHz at 100 °C.

III. The Efficiency of the Refluorescent Filter

The efficiency of the refluorescent filter is one of the most important parameter for its application. The overall efficiency of the system will depend on the reflection efficiency of the potassium vapor filter, the collection efficiency of the entrance lens system, and the collection efficiency of the camera imaging lens. Only the reflection efficiency of the filter is studied here. To estimate the fundamental quantum efficiency of the potassium vapor cell, the fluorescence signal intensity was compared to the scattering intensity from a Lambertian surface. The experiment was set up as shown in figure 6. The collimated Sacher laser beam was sent to the front window of the K vapor cell after passing through an optical chopper and a neutral density filter. The size of the laser beam spot on the cell was roughly 3~5 mm². The fluorescent light was collected by a lens, and sent to a PMT detector. An aperture was used in front of the PMT to ensure that only the fluorescent photons at the potassium vapor cell front surface were detected by the PMT. The PMT signal was passed through a lock-in amplifier and sent to the computer to be analyzed. The wavelength of the Sacher laser was tuned across the resonant line and the fluorescence signal as a function of frequency was recorded at cell cold tip temperatures ranging from 65 °C to 110 °C.

Subsequently the potassium cell was replaced with a Lambertian surface made from fresh MgO smoke, with an estimated scattering efficiency of 98% [12]. The Lambertian surface was located at the same position as the potassium cell's front window and the signal as a function of laser frequency was recorded. The Lambertian surface is used as the reference for our efficiency estimation. Finally, to assure that background was not significant, the laser was blocked and another scan taken. Figure 6 shows the results of these experiments

From the graph it is evident that the fluorescence cell has its highest efficiency at 90 °C cold tip temperature where it reflects nearly 47% compared to the MgO Lambertian surface, leading to a measured refluorescent response of approximately 48% shown in figure 7, which does not take into account the reflection losses at the cells double entrance window. Light passed in and out, so it must pass through eight surfaces compared to the Lambertian scattered light. At 766.5 nm, each surface has reflection losses of 3.7%, leaving 96.3% transmission. That to the eighth power is 74%. So with antireflection coatings, it may be possible to increase the reflectivity by a factor of 1.35 to 65%.

IV. Modulation Transfer Function and the Imaging Capability of the Refluorescent Filter

The imaging capability of an imaging system can be characterized as a modulation transfer function (MTF). The modulation of image is defined as:

$$M = \frac{T_{\max} - T_{\min}}{T_{\max} + T_{\min}}$$

where T_{\max} is the maximum intensity of the image, T_{\min} is the minimum intensity. Since most images have multi spatial frequency components, the modulation for each spatial frequency component can be defined separately.

The image from any real imaging system cannot maintain all the information from the object. Normally, the imaging system has different capability of transferring information at different spatial frequency. The MTF is defined for the imaging system as the capability of transferring different spatial frequency components from the object to the image:

$$MTF(f) = \frac{M_i(f)}{M_o(f)}$$

where $M_i(f)$ is the modulation of the image at frequency f , $M_o(f)$ is the modulation of the object at f .

In order to measure the MTF of the potassium vapor cell as a passband filter, the experiment was set up as shown in figure 8. The beam from a narrow bandwidth laser was expanded and sent through a diffuser as the light source. Ronchi Rulings with numbers of different lines per inch (lpi) were used as the object. A Nikon camera lens set was used to image the Ronchi Ruling on the refluorescent cell. A Pellicle beamsplitter was used to collect the refluorescent photons while passing the image from the object through. A camera with microscopic lens set was used to image the light from the cell. The distortion of the Nikon lens set and the microscopic lens set are negligible at the center of the field of view, compared to the refluorescence cell.

The laser was tuned across the potassium D2 line, and the image on the refluorescent cell only appeared when the laser frequency is at the resonant line. The interference of the reflections from the cell windows was avoided by tilting the cell at a small angle ($< 5^\circ$). A refluorescent image from a 100 lpi Ronchi Ruling is shown in figure 9.

The refluorescent image is digitized and transferred into the frequency space by Fast Fourier Transformation (FFT). The result is plotted in figure 10 (a).

As a reference, a black-write bar pattern with the same frequency of the refluorescent image is generated and transferred to the frequency space as shown in figure 10 (b).

The FFT of a square-wave has discrete peaks in frequency space. The peak at frequency zero is the average intensity of the signal. The first peak near the zero frequency is the intensity of the fundamental frequency, then the 3rd harmonic, 5th harmonic and so on.

The modulation of the image at spatial frequency f_k is given by:

$$M(f_k) = \frac{I_{f_k}}{I_{average}} = \frac{I(f_k)}{I(0)}$$

So the MTF of the refluorescent cell imaging system is:

$$MTF(f_k) = \frac{I_i(f_k) I_o(0)}{I_o(f_k) I_i(0)}$$

Due to the limitation of spatial frequency component of the Ronchi ruling, only two or three point of the MTF can be generated from each Ronchi ruling. In the experiment, Ronchi rulings with 50 lpi, 100 lpi, 150 lpi and 200 lpi were used. All data are put into one graph and shown in figure 11.

From the plot, it can be seen that the spatial frequency response is 50% at 30 cycles per mm. From the model of potassium vapor absorption, the optical depth of potassium vapor at $T_{tip}=100\text{ }^\circ\text{C}$ is roughly $35\text{ }\mu\text{m}$, which means 70% of the at resonant photons are trapped in the first $35\text{ }\mu\text{m}$ after they entered the K vapor. Since the reemission point is random in the area, any image components with finer resolution than this length scale will be blurred. This is consistent with our MTF measurements. Higher values of the MTF at high special frequencies are expected for higher number density of the K vapor, but the quantum efficiency of the refluorescent filter appears to be reduced by the increase of the collisional quenching, most likely with the window.

V. Conclusion

Using the refluorescence feature of the K vapor at the resonant wavelength, it has been shown that an optically thick potassium cell can be used as a passband filter with high imaging capability. It has 1GHz linewidth, and the highest resolution is 30 lines/mm ($33\text{ }\mu\text{m}$). By comparing the refluorescence to a Lambertian surface with known reflectivity, the quantum efficiency of the imaging cell is estimated to be $>60\%$. Unlike the conventional interference filters, the refluorescent filter has a theoretical acceptance solid angle of 2π .

References

- ¹Wynn Wyett and John Reinert, “*Engineering Performance Analysis with plume Spectroscopy*” Threshold: Rocketdyne’s Engineering Journal of Power Technology, 1992.
- ²J.A. Gelbwachs, IEEE Journal of Quantum Electronics 28 (11): 2577-2581, 1992
- ³R.B. Miles, A. Yalin, Z. Tang, S.H. Zaidi, J. Forkey, Journal of Measurement Science and Technologies. Vol. 12, 2001, pp. 442-451
- ⁴Z. Tang, “Infra-red rubidium atomic resonant filters for low wavenumber scattering” Phd Thesis, Department of Mechanical and Aerospace Engineering, Princeton University, June 2001
- ⁵N.D. Finkelstein, W.R. Lempert, and R.B.Miles, Optical Letters 22, P537, 1997
- ⁶Langberg, Naylor, and Hechtsher, Conference on Optical Instruments and Techniques, 1961, London (London, Chapman and Hall 1962).
- ⁷Temirov, Spectrochimica Acta, Part B, Vol. 59, 2004, pp. 677-687
- ⁸N. Bendali, H.T.Duong and J.L.Vialle, Journal of Physics. B: Atomic, Molecular and Optics Physics 11, P4231-4240, 1981
- ⁹D.S. Hughes, P.E. Lloyd, Physical Review 52, P1215-1220, 1937
- ¹⁰E.E. Whiting, Journal of Quantitative Spectroscopy and Radiative Transfer 8, P1379-1384, 1968
- ¹¹Boca Raton, CRC Handbook of chemistry and physics [electronic resource], CRC Press, 1999
- ¹²F. Grum and G. W. Luckey, Applied Optics 7, 11, p2289, 1968

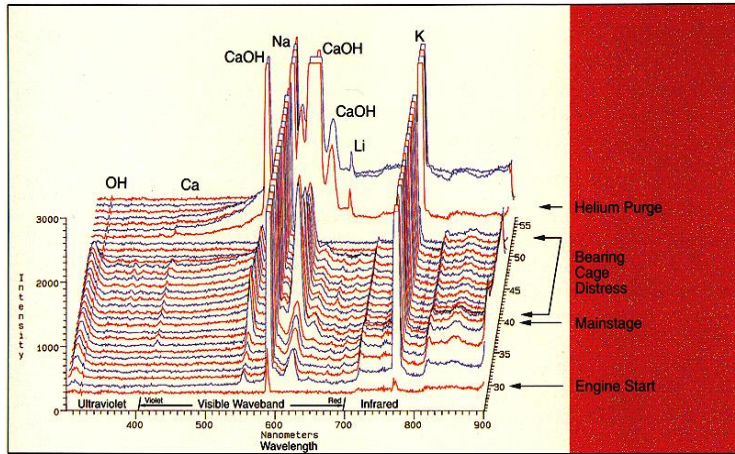


Figure 1. Spectral Features of Missile Plume, 300 – 900 nanometers. [1]

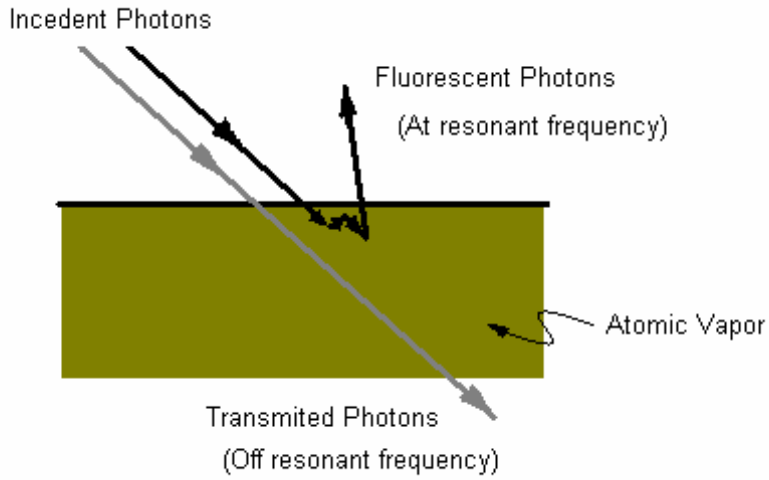


Figure 2. The concept of the refluorescence passband filter

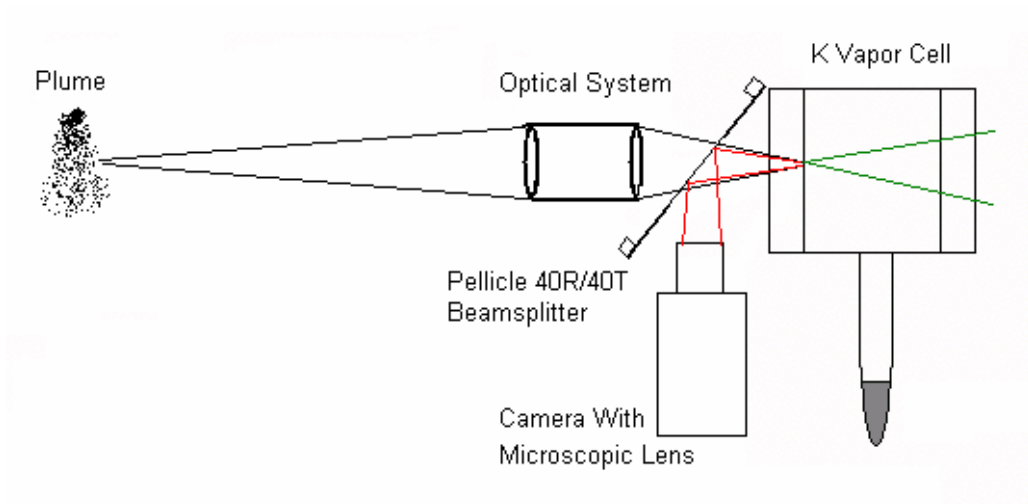


Figure 3. The Conceptual Design.

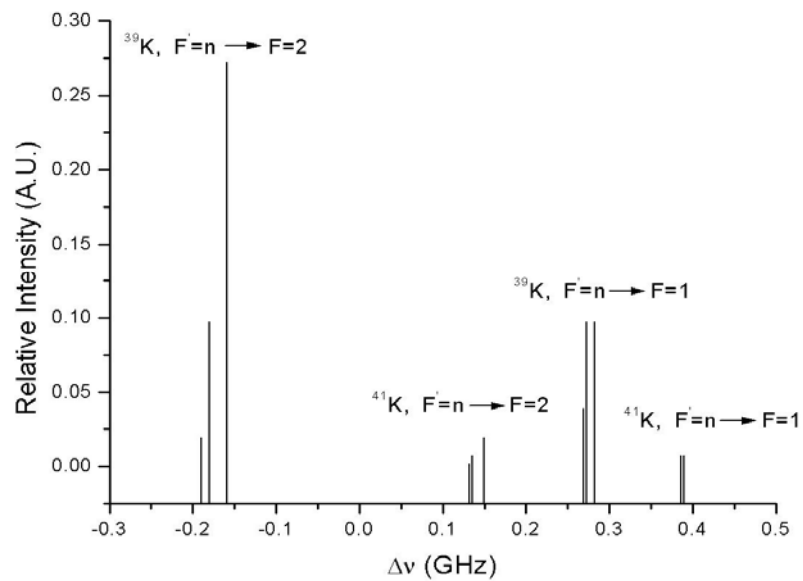


Figure 4. The Hyperfine Structure of potassium D₂ Line.

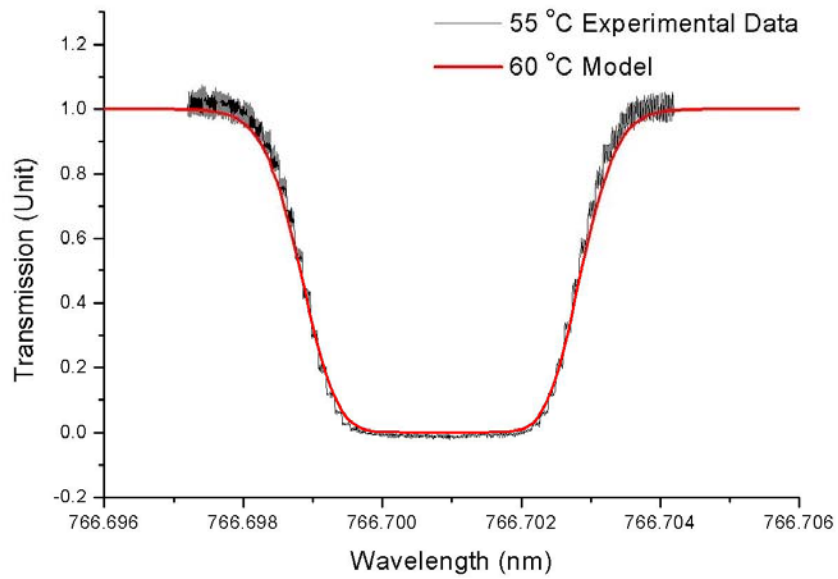
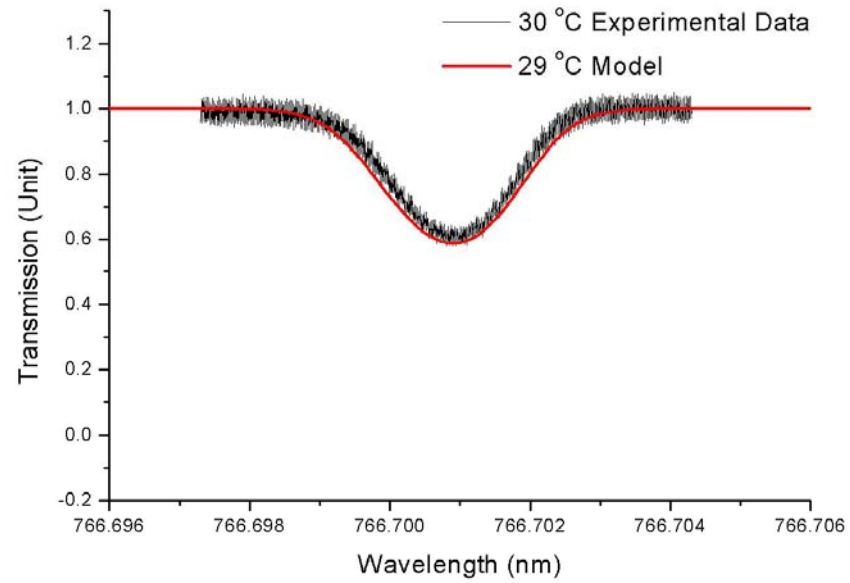


Figure 5. The modeling and measurements of Potassium Cell absorption

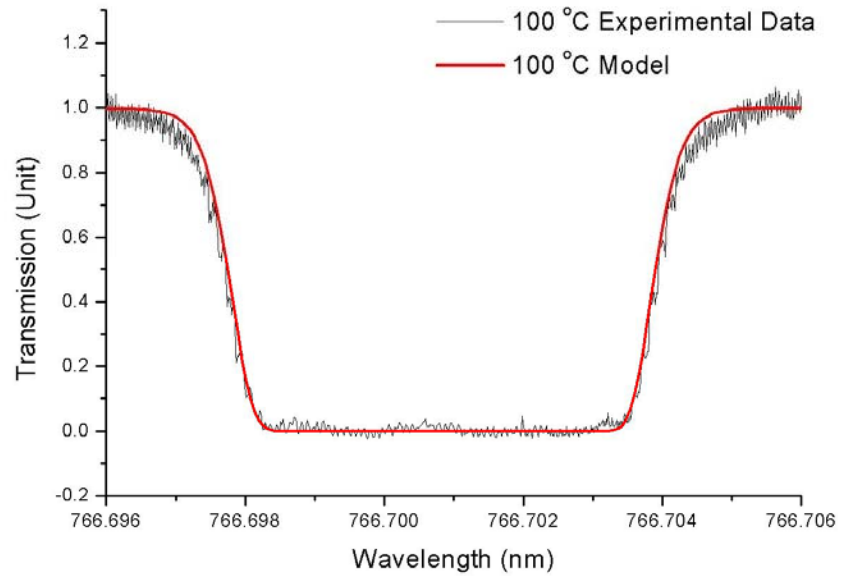


Figure 5. The modeling and measurements of Potassium Cell absorption. (cont.)

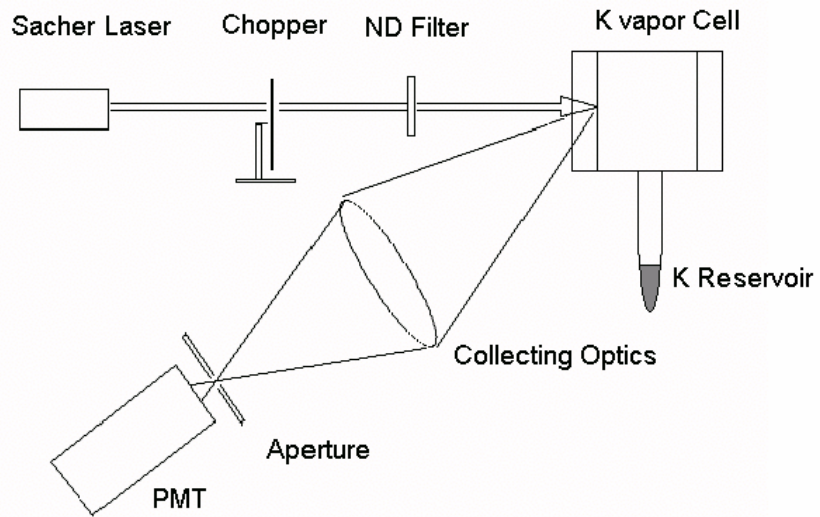


Figure 6. Experimental Setup for the Efficiency measurements.

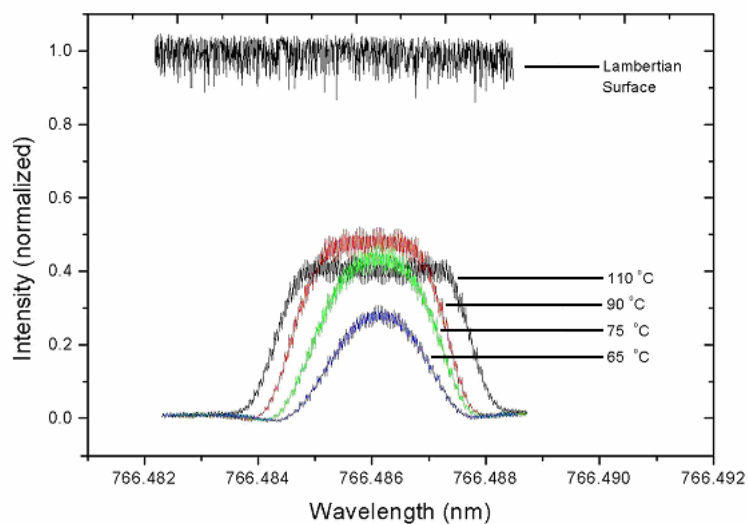


Figure 7. Efficiency measurement results. measurement. Accounting for the reflection losses of the cell's uncoated double window, the refluorescent filter net quantum efficiency is >60%.

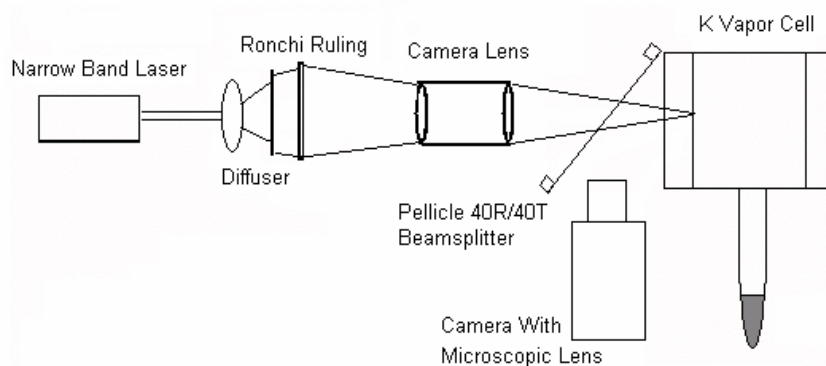


Figure 8. Experimental setup for the MTF measurement.

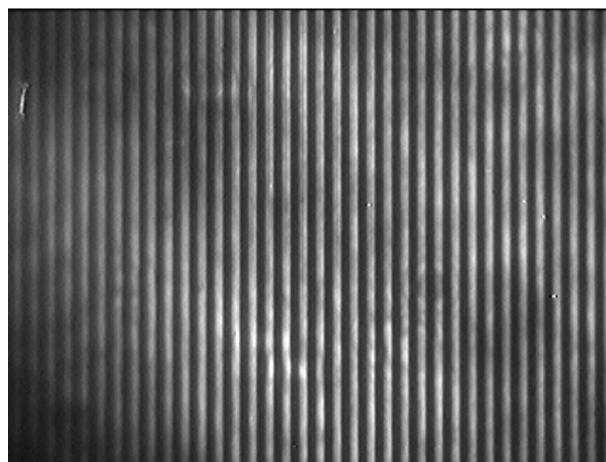
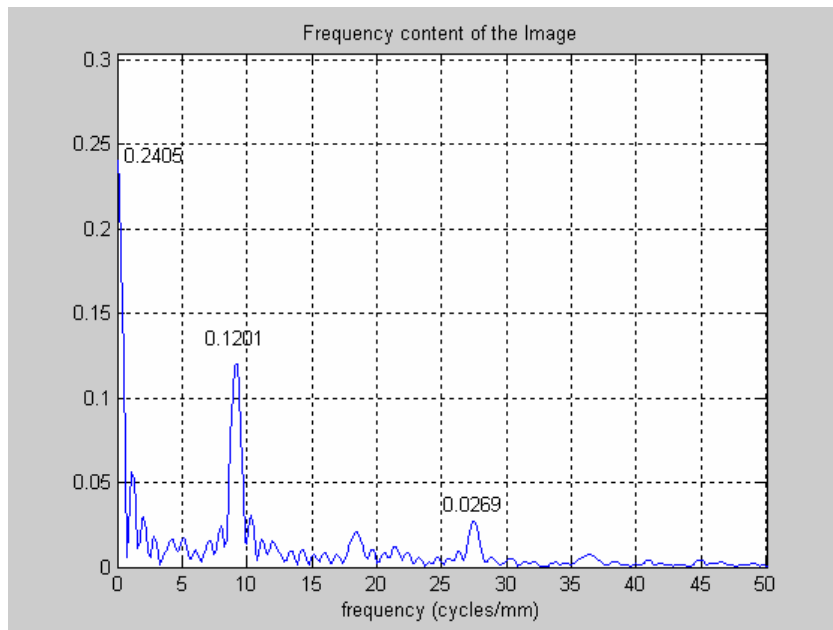
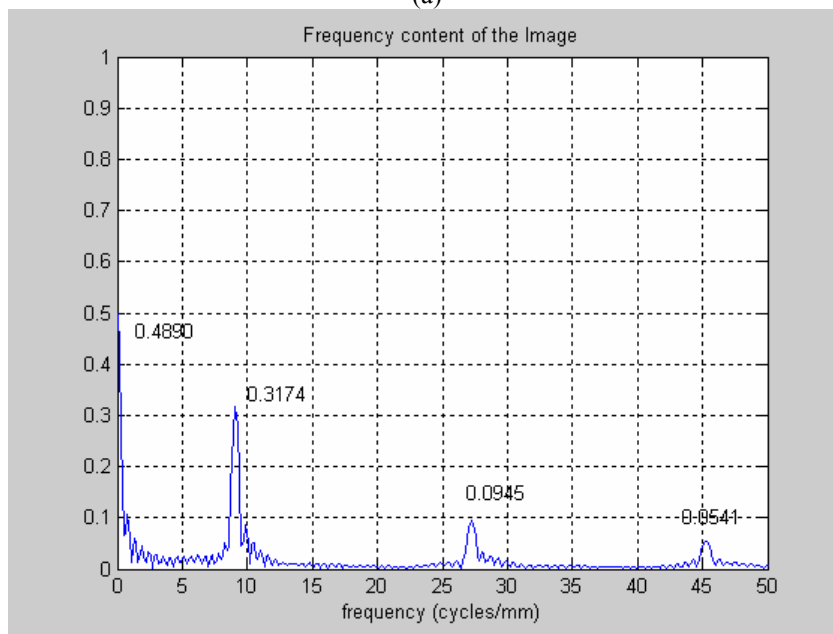


Figure 9. The refluorescent image from the potassium vapor cell with a cold tip temperature of 100°C from a 100 lpi Ronchi Ruling. Line spacing in this image is 110 μ



(a)



(b)

Figure 10. Spatial intensity distribution (cont.) (a) From the refluorescent image in figure 9. (b) From a bar pattern with the same frequency.

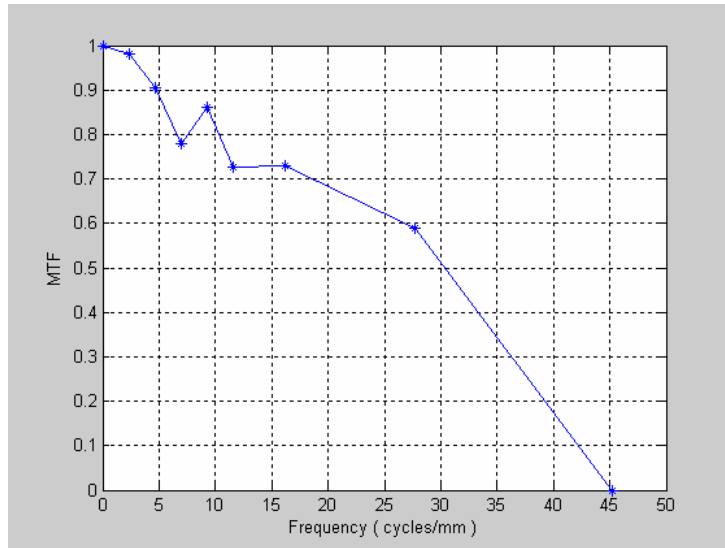


Figure 11. MTF Measurement result for 100⁰C cold tip temperature potassium cell